Geoderma Regional 42 (2025) e00979

Contents lists available at ScienceDirect

Geoderma Regional

journal homepage: www.elsevier.com/locate/geodrs

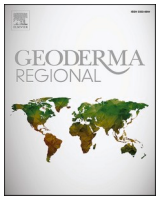

Cashew residue biochar enhances the pore network of cohesive soil in the Brazilian Coastal Tablelands

Jaedson Cláudio Anunciato Mota [a], Emanuela Barbosa dos Santos [a], Alexandre dos Santos Queiroz [a], Odair Pastor Ferreira [b], Antônio Gomes de Souza Filho [c], Laís Gomes Fregolente [c], Francisca Gleiciane da Silva [a], Arthur Prudêncio de Araujo Pereira [a], Helon Hébano de Freitas Sousa [a], Mirian Cristina Gomes Costa [a], Ícaro Vasconcelos do Nascimento [a,*]

[a] Federal University of Ceará (UFC), Soil Science Department, 2977, Av. Mister Hull, Campus do Pici, 60356-001 Fortaleza, CE, Brazil
[b] State University of Londrina (UEL), Department of Chemistry, Highway Celso Garcia Cid (445) - km 380, 86050-482 Londrina, PR, Brazil
[c] Federal University of Ceará (UFC), Department of Physics, Campus do Pici, 60455-900 Fortaleza, CE, Brazil

ARTICLE INFO

Keywords:
Soil conditioners
Soil structure
Soil functionality

ABSTRACT

Soil physical quality is essential for agricultural productivity and environmental sustainability. Cohesive horizons often present high bulk density and low macroporosity, limiting water flow and aeration. This study evaluated the application of biochar derived from cashew residue as a conditioner to improve the physical quality of cohesive soils. We hypothesized that cashew residue biochar enhances soil (macro) porosity, pore connectivity, water retention, and water and airflow in cohesive horizons. The experiment was conducted with five biochar application rates (0, 5, 10, 20, and 40 Mg ha^{-1}) in a randomized design, using disturbed soil samples manually packed into cylinders to ensure consistent bulk density. We analyzed the soil-water retention curve (SWRC), pore size distribution curve (PSDC), air permeability, pore continuity indices, and saturated hydraulic conductivity. Results demonstrated significant improvements in soil structure and pore functionality at higher biochar doses (20–40 Mg ha^{-1}), despite the pore-blocking effect observed at these rates. The 40 Mg ha^{-1} treatment increased macroporosity by 15.3 %, while pore connectivity indices N and Log M rose by 34.2 % and 18.3 %, respectively. Available water improved by 9.1 %, and air permeability increased by 63.3 %, 45.0 %, 20.7 %, and 43.3 % at matric potentials of −6, −10, −33, and −100 kPa, respectively. Saturated hydraulic conductivity also increased by 18 % with the highest dose. These findings demonstrate the potential of cashew residue biochar to enhance the physical quality of cohesive soils, supporting more efficient soil management and sustainable agriculture. Applications between 20 and 40 Mg ha^{-1} are recommended to optimize improvements in soil physical properties.

1. Introduction

The soil performs a wide range of functions within both natural and managed ecosystems. These functions include supporting plant and animal growth, contributing to the maintenance and improvement of water quality, providing mechanical support for buildings and infrastructure, and promoting the health of humans, plants, and animals. Also, it serves as a carbon reservoir that aids in atmospheric carbon sequestration and consequently mitigates climate change; providing a habitat for a vast diversity of organisms; and facilitating nutrient cycling and organic matter decomposition (Karlen et al., 1997; Nascimento et al., 2023; Zhang et al., 2024b).

In this context, the term “soil quality” refers to its capacity to perform these and other functions effectively and sustainably over time (Doran and Parkin, 1994; Seifu and Elias, 2018). This concept arises from the interplay of its physical, chemical, and biological attributes, which together determine the role of soil in the biosphere (Lal, 2016). Soil quality, therefore, is not an isolated or static attribute but rather a holistic state that encompasses the physical structure and the dynamic interplay of elements and (bio)chemical processes within the soil

* Corresponding author.
E-mail address: icaro_agro@hotmail.com (Í.V. do Nascimento).

https://doi.org/10.1016/j.geodrs.2025.e00979
Received 19 November 2024; Received in revised form 12 June 2025; Accepted 13 June 2025
Available online 14 June 2025

(Nascimento et al., 2024). Consequently, soil quality is fundamental to its resilience and its capacity to withstand environmental and anthropogenic pressures, ensuring the continuity of its ecological functions.

From a physical standpoint, particular emphasis is placed on indicators that directly influence plant development — namely, water, oxygen, temperature, and the mechanical resistance (Letey, 1985). Accordingly, a suite of quantitative metrics has been employed to evaluate soil physical quality, including bulk density, total porosity, pore-size distribution, air permeability, hydraulic conductivity, soil penetration resistance, and tensile strength (Arshad and Martin, 2002; Lopes et al., 2024; Nascimento et al., 2024).

Literature reports the occurrence of highly cohesive soil horizons in several parts of the globe. For example, Australia has *hardsetting horizons* characterized by an apedal structure that is hard when dry, with clods that do not break when pressed between the thumb and forefinger but become soft upon wetting (National Committee on Soil and Terrain, 2009). Mullins et al. (1990) highlighted the possibility of similar hardsetting soil behavior occurring in Brazil.

Some soils found in the coastal region of Brazil exhibit limitations in their physical quality due to the presence of pedogenetically densified subsurface horizons — known as cohesive horizons — that impose physical restrictions on root growth, particularly during dry seasons and when these horizons are close to the soil surface (Mota et al., 2018; Nascimento et al., 2024; Oliveira et al., 2020; Queiroz et al., 2023). This horizon leads to considerable costs associated with subsoiling practices in agricultural areas, significantly increasing local production costs (Corrêa et al., 2023). Subsoiling requires heavy machinery with substantial energy demands, can induce traffic-related compaction, and may accelerate soil organic carbon decomposition while disrupting soil aggregates (Ning et al., 2022).

Horizons with cohesive character also limit water and air movement within the soil (Lopes et al., 2024; Menezes et al., 2018). Despite these challenges related to the impediment of water and air flows, the functional behavior of the pore network in these cohesive soils remains largely unexplored. Therefore, a thorough evaluation of pore-space functionality is essential both to gauge the efficacy of soil conditioners, particularly biochar, and to establish their optimal application rates as a sustainable management strategy for these problematic soils. These conditioners can be applied to the soil to depths of up to 0.40 m under conventional farming, and in some instances extend to 0.80 m (Campos et al., 2022).

Biochar, a soil conditioner produced by pyrolyzing biomass under oxygen-limited conditions (Varkolu et al., 2025; Wang and Wang, 2019), is an effective strategy for improving the physical quality of cohesive soils, as its application can reduce soil cohesion (Zong et al., 2014). Biochar is C-rich material characterized by a high specific surface area and a high density of negatively charged surfaces, which allows it to adsorb water and nutrients for plant use (Yang et al., 2019). Biochar enhances soil aggregation and improves porosity (total porosity and pore connectivity), aeration, and hydraulic conductivity. It also stimulates microbial activity, reduces soil cohesion and mechanical resistance, and contributes to carbon sequestration due to the high recalcitrance of its carbon structure (Elkhlifi et al., 2023; Li and Tasnady, 2023; Luo et al., 2023; Nascimento et al., 2023).

Beyond its local availability (Oliveira and Ipiranga, 2011), cashew residue biochar offers distinctive agronomic advantages that justify its use as a soil amendment. Due to its high specific surface area and porous structure, this material can improve soil water retention, promote nutrient adsorption, and enhance cation exchange capacity, especially in sandy or degraded soils (Fregolente et al., 2023; Nascimento et al., 2023, 2024). Moreover, the cashew residue biochar supports the sustainable management of regional agro-industrial waste by adding value to by-products that are typically underutilized. These characteristics make cashew residue biochar a promising strategy for improving soil quality and promoting the circular economy.

This study is among the first to specifically evaluate the effects of biochar derived from cashew processing residues on the physical properties of cohesive soils. While biochar has been extensively studied in various soil types (Blanco-Canqui, 2017), there is a significant knowledge gap regarding its influence on densified, cohesive horizons common in tropical regions. Our research addresses this gap by investigating how cashew residue biochar impacts pore connectivity, water retention, and air permeability in these challenging soil conditions, providing novel insights for sustainable soil management.

Thus, we hypothesize that applying biochar derived from cashew processing residues improves soil (macro)porosity, pore connectivity, water retention, and airflow, thereby enhancing the physical quality of cohesive soils. We aimed to identify the most effective biochar dosage for these improvements.

2. Material and methods

2.1. Soil sampling

The soil sampling was conducted in an experimental area at the Federal University of Ceará, located in Fortaleza, Ceará, Brazil. Fortaleza has a tropical wet-dry climate, classified as Aw according to Koppen (1918). The sampled soil (Fig. 1, 546,528.0 E, 9586059.0 N – UTM 24S) was classified as a *Argissolo Amarelo Eutrocoeso típico* (Santos et al., 2018), corresponding to a Haplic Lixisol (IUSS Working Group WRB, 2022).

The studied horizon is classified as sandy clay, with a textural composition of 45.9 % sand, 10.1 % silt, and 44.0 % clay, as detailed in Table 1. Soil samples with deformed structure were collected from the center of the Bt1 horizon (0.96–1.45 m depth, with cohesive character) for the preparation of soil cylinders, as detailed in Nascimento et al. (2024).

2.2. Experimental design, biochar production and preparation of soil cylinders

The experimental design was completely randomized, incorporating five distinct biochar application rates as treatments and five replicates per treatment, resulting in 25 experimental units consisting of metallic rings filled with soil (approximately 100 cm^3, with an internal height and diameter of about 5 cm). The treatments were labeled as B0 (0 Mg ha^{-1}), B5 (5 Mg ha^{-1}), B10 (10 Mg ha^{-1}), B20 (20 Mg ha^{-1}), and B40 (40 Mg ha^{-1}).

Cashew bagasse was selected due to its regional availability to produce the biochar. The bagasse was dried in an oven at 40 °C for 24 h, then ground and sieved through a 2 mm mesh. Biochar production involved slow pyrolysis in a tubular furnace (FTHI/20, EDG) at 550 °C for 90 min under a moderate nitrogen flow. The particle size distribution of the biochar was determined by dry sieving using a set of sieves with mesh openings of 1.00 mm, 0.50 mm, 0.25 mm, 0.105 mm, and 0.053 mm. The material was separated into the following size fractions: 2.00–1.00 mm, 1.00–0.50 mm, 0.50–0.25 mm, 0.25–0.105 mm, 0.105–0.053 mm, and < 0.053 mm, with each fraction expressed as a percentage of the total sample. The biochar characteristics are detailed in Table 2.

Before assembling the cylinders, the disturbed soil samples were air-dried until they reached equilibrium with the ambient moisture, then sieved through a 2 mm mesh to obtain air-dried fine earth (ADFE). The soil cylinders were prepared using this ADFE, and the biochar was obtained from cashew processing residues according to the specified application rates. Before preparing the samples in metallic rings, the ADFE was thoroughly mixed with the biochar. This mixing was done by placing the ADFE and biochar in a plastic bag, sealing the bag, and shaking it to ensure a uniform mixture.

A set of samples was prepared to obtain the soil-water retention curve, pore size distribution curve, air permeability, and pore continuity indices. A second set was designated for evaluating saturated hydraulic

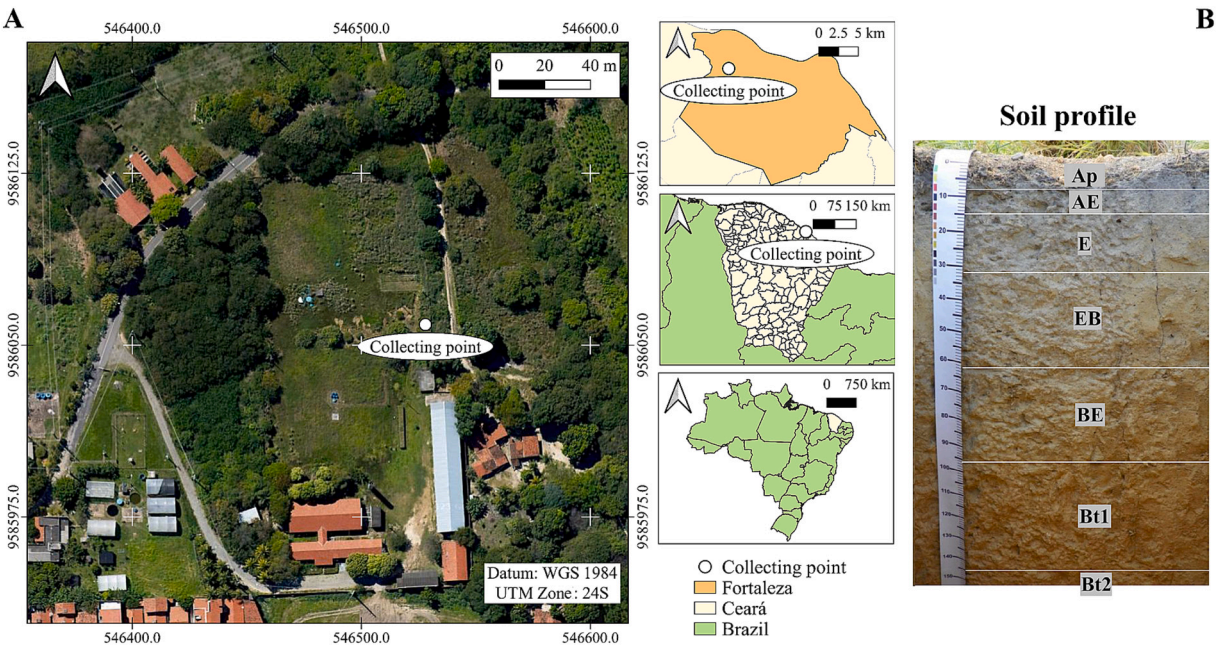

Fig. 1. Location of the sampling site in Fortaleza, Ceará, Brazil (A). Profile of the *Argissolo Amarelo Eutrocoeso típico* (Haplic Lixisol) (B). Map prepared by Nascimento et al. (2024). Soil profile photo credits: Vieira (2013).

Table 1
Soil characterization.

Horizon	Depth (cm)	Exchangeable cations ($cmol_c\ kg^{-1}$)						SB	CEC	BS (%)	pH	Granulometric fractions (%)		
		Ca	Mg	K	Na	Al	H					Sand	Silt	Clay
Ap1	0–8	3.0	4.4	0.36	0.37	0.2	2.0	8.13	10.33	79	6.0	82.6	10.9	6.5
AE	8–15	2.0	3.8	0.21	0.37	0.2	1.2	6.39	7.79	82	6.2	82.3	9.0	8.7
E	15–32	1.4	2.8	0.24	0.36	0.4	1.8	4.79	6.99	69	6.3	81.0	6.6	12.4
EB	32–62	1.4	3.2	0.30	0.43	0.4	1.8	5.33	7.53	71	6.3	70.6	7.8	21.6
BE	62–96	2.2	2.0	0.39	0.41	0.6	1.5	5.00	7.10	70	6.3	61.4	9.4	29.2
Bt1	96–145	1.6	3.8	0.40	0.43	0.6	1.6	6.23	8.43	74	6.3	45.9	10.1	44.0
Bt2	145–190+	1.8	3.0	0.17	0.46	0.4	1.6	5.43	7.43	73	6.4	47.9	10.8	41.3

SB – Sum of bases. CEC – Cation exchange capacity. BS – Base saturation. pH measured in water. Source: Vieira (2013).

Table 2
Biochar characterization.

Variables	Values
Ganulometry	–
1.0 to 2.0 mm (%)	31.46
1.0 to 0.5 mm (%)	38.38
0.5 to 0.25 mm (%)	19.12
0.25 to 0.105 mm (%)	8.54
0.105 to 0.053 (%)	1.95
< 0.053 mm (%)	0.55
[1]Specific surface area ($m^2\ g^{-1}$)	70.00
[1]C (%)	80.10
[1]H (%)	2.50
[1]N (%)	2.80
[01]S (%)	0.20
[1]O (%)	10.80
[1]Ash (%)	3.60
[1]O/C Atomic ratio	0.10
[1]H/C Atomic ratio	0.38

[1] Source: Fregolente et al. (2023).

conductivity. The biochar was thoroughly mixed with the soil before sample preparation. All samples, including the control and biochar-amended treatments, were then packed to the same initial bulk density (1.55 Mg m^{-3}), corresponding to the bulk density of the soil horizon from which the samples were collected. This procedure ensured uniform initial conditions across treatments, allowing any changes in soil structure to be attributed solely to the effect of biochar addition rather than to differences in initial bulk density.

The samples were manually packed into the PVC cylinders to achieve a uniform bulk density (Fig. 2). The packing process was carried out in three successive layers. Each layer was carefully added and compacted using consistent manual pressure to ensure homogeneity throughout the profile. The manual compaction was standardized across all samples to maintain experimental consistency.

All experimental units underwent ten cycles of wetting and drying to manifest the cohesive character and to enable the biochar doses to induce detectable changes in soil structure. One cycle was conducted each week from August 23, 2021, to November 1, 2021, spanning a total of ten weeks. Each cycle comprised two days of wetting followed by five days of air drying. Each Monday at 2 PM, the samples were placed on sponges saturated with distilled water to moisten by capillarity. Subsequently, every Wednesday at 2 PM, the samples were removed from the sponges and left to air-dry in plastic trays until the following Monday. The laboratory temperature was 28.8 °C (±2.1 °C) throughout the cycles.

2.3. Analyzed attributes

In this section, we selected a targeted set of soil physical parameters to elucidate the multifaceted effects of biochar amendment. These

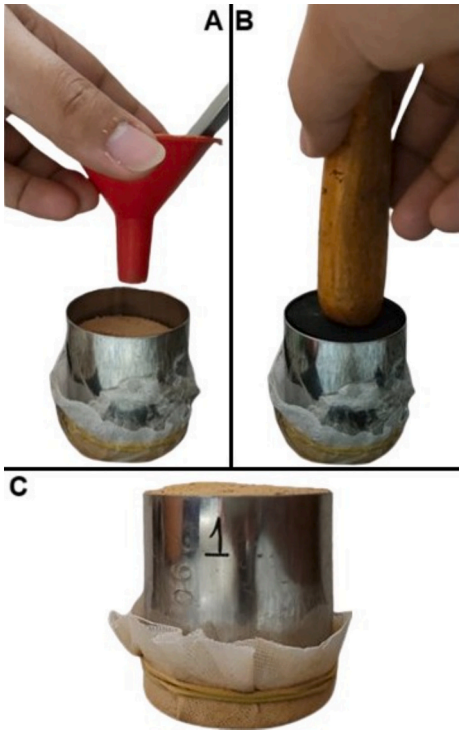

Fig. 2. Sample Assembly Procedure: (A) Material addition, (B) manual compaction, and (C) assembled specimen.

parameters were grouped according to the primary functional impacts of biochar, as outlined below:

2.3.1. Effects on water retention and plant-available water

2.3.1.1. Soil-water retention curve (SWRC) and pore size distribution curve (PSDC). The SWRC was obtained using soil cylinders. In this procedure, the moisture at saturation was considered equivalent to the total porosity (α, $m^3\ m^{-3}$). For low matric potential points (−2, −6, and − 10 kPa), a Haines funnel was used to establish equilibrium between the matric potential applied and the soil moisture. For the remaining points (−33, −100, −300, −700, and −1500 kPa), equilibrium was achieved using a Richards pressure plate extractor (Soil Moisture Equipment Corp.) (Klute, 1986). Subsequently, the mathematical model proposed by van Genuchten (1980) (Eq. 1) was fitted to the experimental data.

$$\theta = \theta_r + \frac{\theta_s - \theta_r}{[1 + (\alpha|\Psi_m|)^n]^m} \quad (1)$$

where θ represents the volumetric moisture ($m^3\ m^{-3}$); θ_r and θ_s are, respectively, the residual and saturation moisture ($m^3\ m^{-3}$); Ψ_m is the soil matric potential (kPa); α is a scaling parameter associated with the matric potential axis (kPa^{-1}); and m and n are model fitting parameters related to the curve shape. The model was fitted using the SWRC – Soil Water Retention Curve software (Dourado-Neto et al., 2000).

Using the SWRC, the pore size distribution was assessed from Ψ_m = 0 to −1500 kPa. To achieve this, the moisture was derived as a function of the matric potential ($d\theta/d\Psi_m$) from the function $\theta = f(\Psi_m)$. The peak of the resulting curve, known as PSDC, indicates the matric potential corresponding to the most frequent pore size in the soil.

2.3.2. Pore continuity and blockage mechanisms

2.3.2.1. Pore continuity indices and blocked porosity. In this procedure, the soil air permeability values (K_{air}) were correlated with the aeration porosity (ε_{ar}) using the Kozeny-Carman equation, similar to Ahuja et al. (1984), as presented in Eq. (2),

$$K_{air} = M\varepsilon_{air}^{N} \quad (2)$$

where M (intercept) and N (slope) are empirical constants. The exponent N is considered a pore continuity index, as it reflects the increase in K_{air} with the rise in ε_{air}, or a reduction in pore tortuosity, with an increase in the area available for air flow. The ε_{air} was calculated as the difference between total porosity and volumetric moisture (θ) equilibrated at matric potentials of −2, −6, −10, −33, and −100 kPa.

Eq. (2), when converted into its logarithmic form, results in Eq. (3),

$$log K_{air} = logM + N log\varepsilon_{air}. \quad (3)$$

From the linear regression between $log\ \varepsilon_{ar}$ and $log\ K_{air}$ (Presented in the results section), the values of M and N were estimated. The intercept of the linear line with the abscissa can be used as a measure of the blocked porosity (ε_b), which represents the ε_{ar} value below which airflow through the soil ceases. Based on Eq. (3), ε_b is expressed by Eq. (4),

$$\varepsilon_b = 10^{(-logM)/N} \quad (4)$$

2.3.3. Integrated air and water flow enhancements

2.3.3.1. Air permeability (K_{air}). K_{air} was determined using the pressure decay method (Kirkham, 1947; Neves et al., 2007; Silva et al., 2009; Silveira et al., 2011). For this purpose, samples with moisture equilibrated at matric potential of −2, −6, −10, −33, and − 100 kPa were used. The procedure involved passing a quantity of air corresponding to a pressure of 1 kPa through each sample. The pressure decay over time was then measured electronically until the pressure within the sample equilibrated with atmospheric pressure. These operations were performed using the PermeAr software (Silveira et al., 2011). The K_{air} was calculated using Eq. (5),

$$K_{air} = \frac{L\eta V}{AP_{atm}} \times |S| \quad (5)$$

where K_{air} is the air permeability coefficient (m^2); V is the volume of air passing through the cylinder (m^3); η is the air dynamic viscosity of air (Pa s); L is the height of the volumetric ring (m); A is the cross-sectional area of the soil sample (m^2); P_{atm} is the atmospheric pressure (Pa); and S is the slope of the linear regression of pressure (ln of pressure) as a function of time. The K_{air} results have been converted from m^2 to μm^2 to ensure consistency with the standard units used in soil-physics literature.

2.3.3.2. Saturated soil hydraulic conductivity (K_s). To measure this attribute, a cylinder with dimensions of 25 cm in height and 50 cm in diameter was affixed to the top of the cylinder containing the sample to be analyzed. The test was conducted using pre-saturated samples, following the constant head permeameter method (Youngs, 2000). The principle of this method is to maintain a constant water head over the samples, while simultaneously collecting the volume of water drained from the bottom of the cylinder at known time intervals. Then, K_s was calculated according to Darcy's law,

$$q = -K_s\frac{\Delta\Psi}{L} \quad (6)$$

where q is the water flux density ($m\ s^{-1}$); K_s is the saturated soil hydraulic conductivity ($m\ s^{-1}$); and $\Delta\Psi\backslash L$ is the potential gradient ($m\ m^{-1}$), which physically represents the force driving the water flow. The negative sign indicates that the direction of movement is opposite to the gradient.

2.4. Statistical analyses

All response variables were screened first for normality using the Shapiro–Wilk test (α = 0.05) and homoscedasticity using Levene's test (α = 0.05). When both assumptions were satisfied, one-way ANOVA was conducted, and means were compared via Tukey's test (α = 0.05). Linear regressions between soil attributes and biochar dose were performed only when residuals met ANOVA assumptions. All analyses were carried out in SAS® Studio.

3. Results

3.1. Effects on water retention and plant-available water

In the parameters of the van Genuchten (1980) equation, a significant difference was observed only for the parameter θs, with the 20 and 40 Mg ha^{-1} doses standing out (Table 3). Regarding α, a scaling parameter of the matric potential axis (van Lier and Pinheiro, 2018), as well as the parameters m and n, related to the shape of the curve (Nascimento et al., 2018b), was not statistically different between the treatments.

Examining the SWRC (Fig. 3, primary axis), it is notable that for the 20 and 40 Mg ha^{-1} doses, there was an increase of 15.3 % in soil moisture in the range corresponding to macroporosity, i.e., from saturation ($\Psi m = 0$) to $\Psi m = -6$ *kPa* (Reichardt and Timm, 2020). In the PSDC (Fig. 3, secondary axis), for the B20 and B40 treatments, the most frequent pore size is associated with a matric potential of −1.96 kPa, corresponding to a pore of approximately 150 μm in diameter.

Plant-available water, calculated as the difference between soil moisture at field capacity ($\Psi_m = -33$ *kPa*) and at the permanent wilting point ($\Psi m = -1500$ *kPa*), showed only minor variation, being 0.055 m^3 m^{-3} in the control treatment and 0.060 m^3 m^{-3} at the highest biochar dose (40 Mg ha^{-1}), corresponding to a 9.1 % increase in available water compared to the control treatment.

3.2. Pore continuity and blockage mechanisms

The highest N value (1.5093) was observed at the 40 Mg ha^{-1} dose (Fig. 4E), representing a 34.2 % increase compared to the control (1.2333) (Fig. 4A). Additionally, the maximum *Log M* values were recorded at the 20 and 40 Mg ha^{-1} doses (2.6028 and 2.6460, respectively) (Fig. 4D and E), corresponding to increases of 16.4 % and 18.3 % relative to the control (2.2362).

Regarding blocked porosity (εb), there was a trend of increasing values with higher biochar doses, with the highest εb observed at the 40 Mg ha^{-1} treatment – 60.3 % higher than the control (Fig. 5A and B).

3.3. Integrated air and water flow enhancements

An increase in the area available for air flow is displayed with the application of the tested biochar (Fig. 7), except under conditions near saturation ($\Psi_m = -2$ *kPa*, Fig. 7A). A biochar dose of 40 Mg ha^{-1} was found to be the most effective in enhancing this attribute (Fig. 6).

Table 3
Parameters of the van Genuchten (1980) model for the evaluated treatments. Means followed by the same lowercase letter in the column do not differ according to Tukey test at 5 % significance.

Treatment	Parameters				
	α (kPa^{-1})	m	n	θr (cm^3 cm^{-3})	θs (cm^3 cm^{-3})
B0	0.225 a	0.429 a	1.758 a	0.153 a	0.417 b
B5	0.229 a	0.416 a	1.718 a	0.155 a	0.418 b
B10	0.221 a	0.429 a	1.755 a	0.158 a	0.421 ab
B20	0.297 a	0.387 a	1.634 a	0.157 a	0.425 a
B40	0.297 a	0.381 a	1.619 a	0.153 a	0.424 a

Except for the condition nearest saturation ($\Psi m = -2$ *kPa*, Fig. 7A), the trend of increasing air permeability with higher biochar doses was statistically significant (Figs. 6B, C, D, and E). Compared to the control, K_{air} increased by 63.3 %, 45.0 %, 20.7 and 43.3 % at matric potentials of −6, −10, −33 and − 100 kPa, respectively, with a dose of 40 Mg ha^{-1} (Fig. 6).

In terms of K_s, the highest value was recorded for the 40 Mg ha^{-1} biochar dose (Fig. 8A), which was significantly different from the control, indicating that the 40 Mg ha^{-1} dose significantly enhanced soil hydraulic conductivity compared to the unamended soil. An upward trend in K_s was observed, with an estimated 18 % increase compared to the control treatment when the soil was amended with biochar at a dose of 40 Mg ha^{-1} (Fig. 8B).

4. Discussion

It is important to note that the physical and chemical properties of biochar—and consequently its effects on soil structure and functionality—can vary widely depending on the original feedstock and pyrolysis parameters such as temperature and residence time (Nascimento et al., 2023). Therefore, the improvements and trade-offs observed in this study with cashew-residue biochar may differ when using biochars produced from other biomass sources or under different pyrolysis conditions, highlighting the need for context-specific evaluation and cautious extrapolation of these findings.

4.1. Effects on water retention and plant-available water

van Genuchten (1980) parameters α, m and n remained statistically equivalent across treatments, demonstrating that biochar addition preserves the intrinsic pore–water retention relationships. Instead, the reduction in bulk density induced by cashew-residue biochar points to an enlargement of macropore domains, which in turn drives the observed increase in total porosity. These findings confirm that biochar acts primarily as a structural ameliorant, enhancing pore architecture without altering the fundamental retention characteristics of cohesive soils (Nascimento et al., 2024; Singh et al., 2022; Verheijen et al., 2019).

The statistical similarity of parameters α, m, and n (Table 3) indicates that the shapes of the SWRC were comparable (Jorge et al., 2010). The primary difference was observed in the parameter θs, which was significantly higher in the biochar treatments due to increased total and macroporosity. The observed increase in soil moisture within the macroporosity range (from saturation to $\Psi_m = -6$ *kPa*) for the B20 and B40 treatments (Fig. 3, main axis), further confirms the enhancement in macroporosity resulting from biochar application. This effect is distinctly illustrated by the orange area in the PSDC (Fig. 3, secondary axis), highlighting the increased macroporosity. An advantage of the PSDC is that it facilitates the evaluation of soil structure even when water retention curves are very similar, as is the case in this experiment (Nascimento et al., 2018a).

It is noteworthy that the most frequent pore size for the B20 and B40 treatments corresponds to approximately 150 μm in diameter (Fig. 3, main axis). Additionally, there was a trend of reduced air permeability at a matric potential of −2 kPa (Fig. 7A) and increased blocked porosity (Fig. 5B) when biochar was applied, with these effects being more pronounced at the higher doses (20 and 40 Mg ha^{-1}). However, the higher proportion of pores with a diameter of 150 μm may have offset the obstruction effect in these treatments, such that the trend of reduced air permeability at −2 kPa was not statistically significant (Fig. 7A). Another factor that may have offset this obstruction is the increased pore connectivity (Fig. 4) with the increase in biochar dose, which facilitates gas exchange processes (Alencar et al., 2016).

It is worth noting that while the similarity in the shape of the SWRC indicates comparable water retention properties despite the biochar application, the increase in plant-available water when comparing the B0 (control) treatment with B40 was 9.1 %. Similar results, in Brazilian

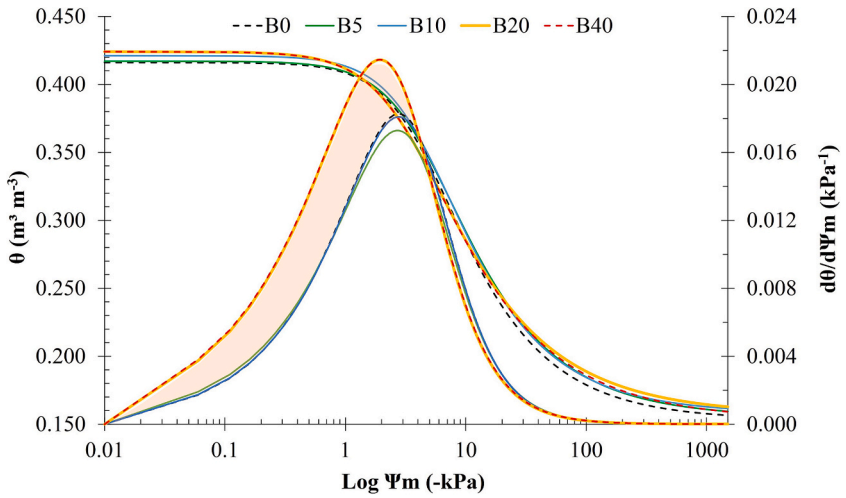

Fig. 3. Soil-water retention curve (primary axis) and pore size distribution curve (secondary axis) for the evaluated treatments. The orange-shaded area indicates the increase in macroporosity in the B20 and B40 treatments.

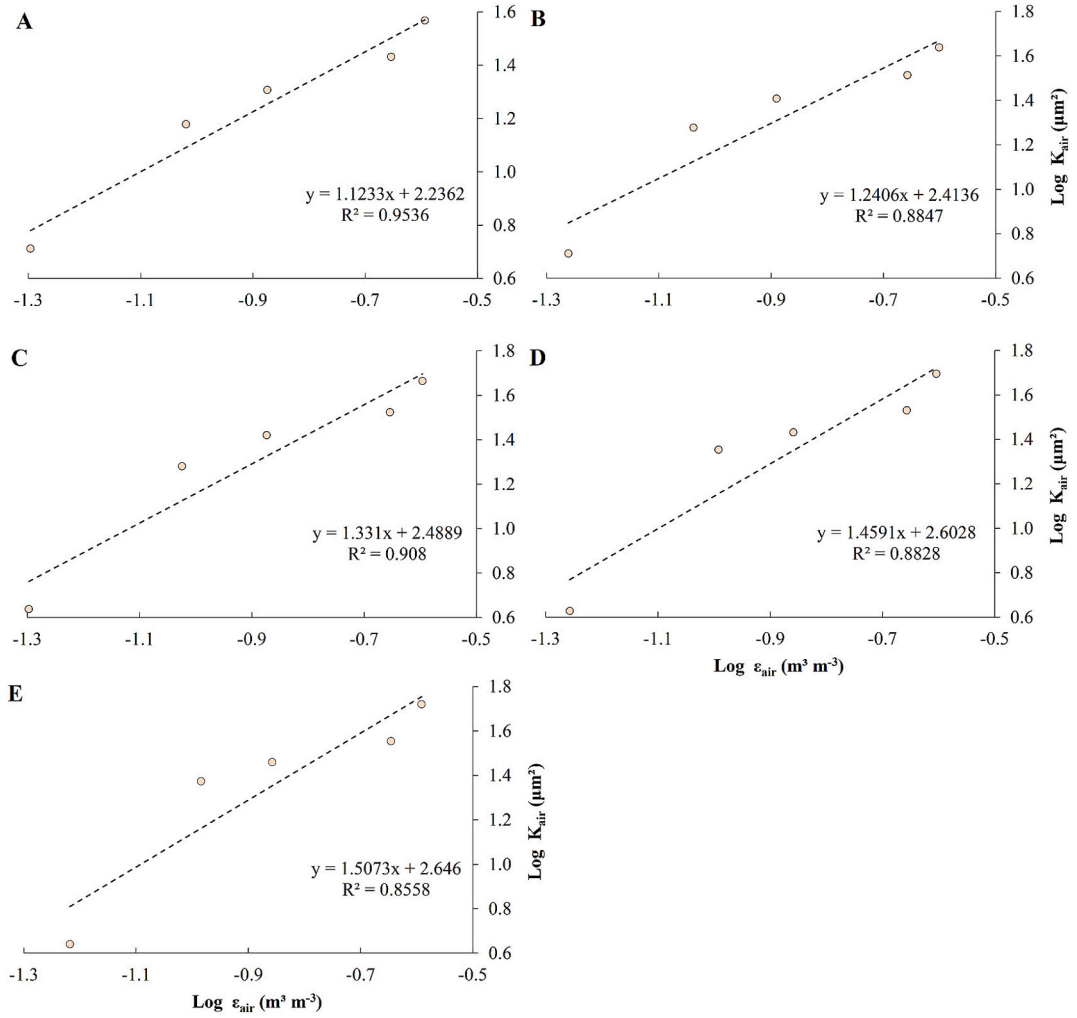

Fig. 4. Linear regression of log ε_{ar} versus log K_{air} under biochar doses of 0 (A), 10 (B), 20 (C) and 40 t ha^{-1} (D) (n = 5). The intercept (Log M) and slope (N) serve as pore continuity indices.

soils, were related by Torres et al. (2024) and Mendes et al. (2021). This trade-off indicates not only improved water availability but also a reduction in cohesion among soil constituents, enhancing the soil's permissiveness to plant root growth, as the cohesive horizon becomes less resistant when moist (Santos et al., 2018).

The predominance of coarser biochar particles (>250 µm; ~97.5 %;

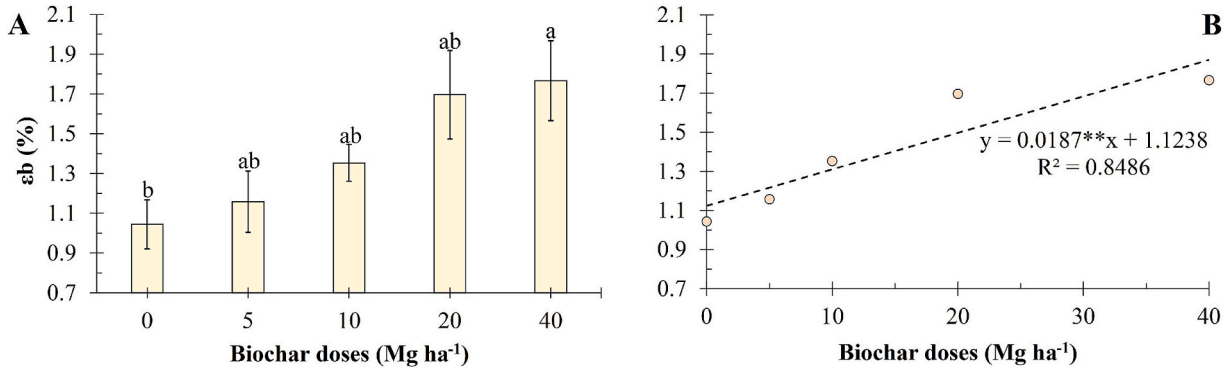

Fig. 5. Blocked porosity (ε_b) as a function of biochar doses (A) (n = 5). Regression between ε_b and biochar doses (B). Means followed by the same letter do not differ according to Tukey test at a 5 % significance level. The bars represent the standard error of the mean. **Significant at the 1 % probability level.

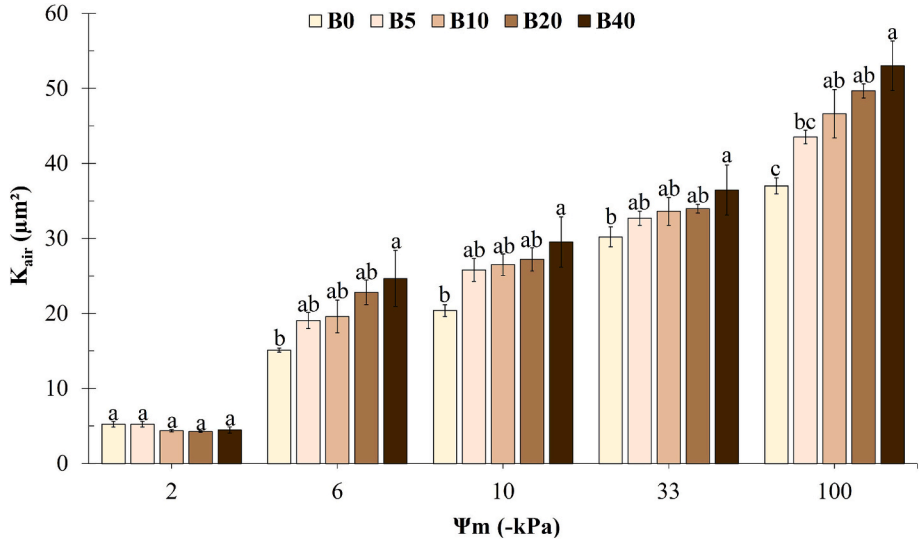

Fig. 6. Air permeability (K_{air}) of soil samples equilibrated at matric potentials of −2, −6, −10, −33 and −100 kPa under biochar doses of 0 (B0), 10 (B10), 20 (B20) and 40 t ha^{-1} (B40) (n = 5). Within each matric potential, means bearing the same letter do not differ significantly according to Tukey' test at α = 0.05. Error bars represent the standard error of the mean.

Table 2) with only 8.54 % in the 105–250 µm range suggests that the pronounced water-retention gains reported Duarte et al. (2019) for the finest fraction (<150 µm) may be attenuated in our system. Nonetheless, because the majority of our biochar still falls within the 0.25–2 mm window shown to enhance total porosity and shift pore-size distribution toward increased macro- and mesoporosity, we anticipate meaningful improvements in aeration and hydraulic conductivity (See topic 4.3) (Duarte et al., 2019).

Additionally, the positive effect on water retention properties should not be overlooked for agricultural soils, given the growing need for efficient water resource management due to scarcity. Although this increase is modest, it is relevant because the effect of biochar on available water is generally less pronounced in clayey soils compared to sandy soils (Edeh et al., 2020; Razzaghi et al., 2020), as it may be mitigated by the clay fraction (Santos, 2021). However, it is important to note that the potential for clay expansion-driven mitigation of biochar effects on water retention depends strongly on mineralogical composition. While clayey soils dominated by 2:1 expansive minerals (e.g., smectite) may develop macropores through shrink–swell behavior and crack formation under drying and wetting cycles (Ahlersmeyer et al., 2025; Yang et al., 2025), this mechanism is less prominent in soils with 1:1 kaolinitic mineralogy, such as the one studied here, due to their low shrinkage potential. Therefore, in this context, biochar-induced improvements in soil structure and water retention become particularly relevant.

4.2. *Pore continuity and blockage mechanisms*

Higher values of *N and Log M* imply an enhancement in the connectivity of the pore network, with a greater number of pores contributing to gas fluxes (Alencar et al., 2016). This explains the increased soil K_{air} observed in treatments with biochar application (Fig. 6). Therefore, the application of the tested biochar resulted in improved pore connectivity and air permeability, enhancing the physical quality of the cohesive horizon, which inherently exhibits restrictions to gas movement (Marques et al., 2021; Menezes et al., 2018; Mota et al., 2018; Queiroz et al., 2023).

Regarding the higher blocked porosity value compared to the control in the B40 treatment (Fig. 5A), it is relevant to note that biochar particles have the potential to occlude soil pores – particularly at high application rates. As seen in Fig. 7A, increasing the biochar dose showed a trend – though not statistically significant – toward reduced K_{air} at a matric potential of −2 kPa. The increase in blocked porosity due to the addition of particulate material to the soil has also been reported by Alencar et al. (2016). Fine biochar particles can block soil macropores (Blanco-Canqui, 2017). Thus, the tested biochar particles occluded pores with diameters of 150 µm or greater, resulting in decreased gas flux at this matric potential – with an increase in blocked porosity, i.e., the proportion of pores not participating in convective processes. However, this increase had minimal effects on K_{air} in response to the increased

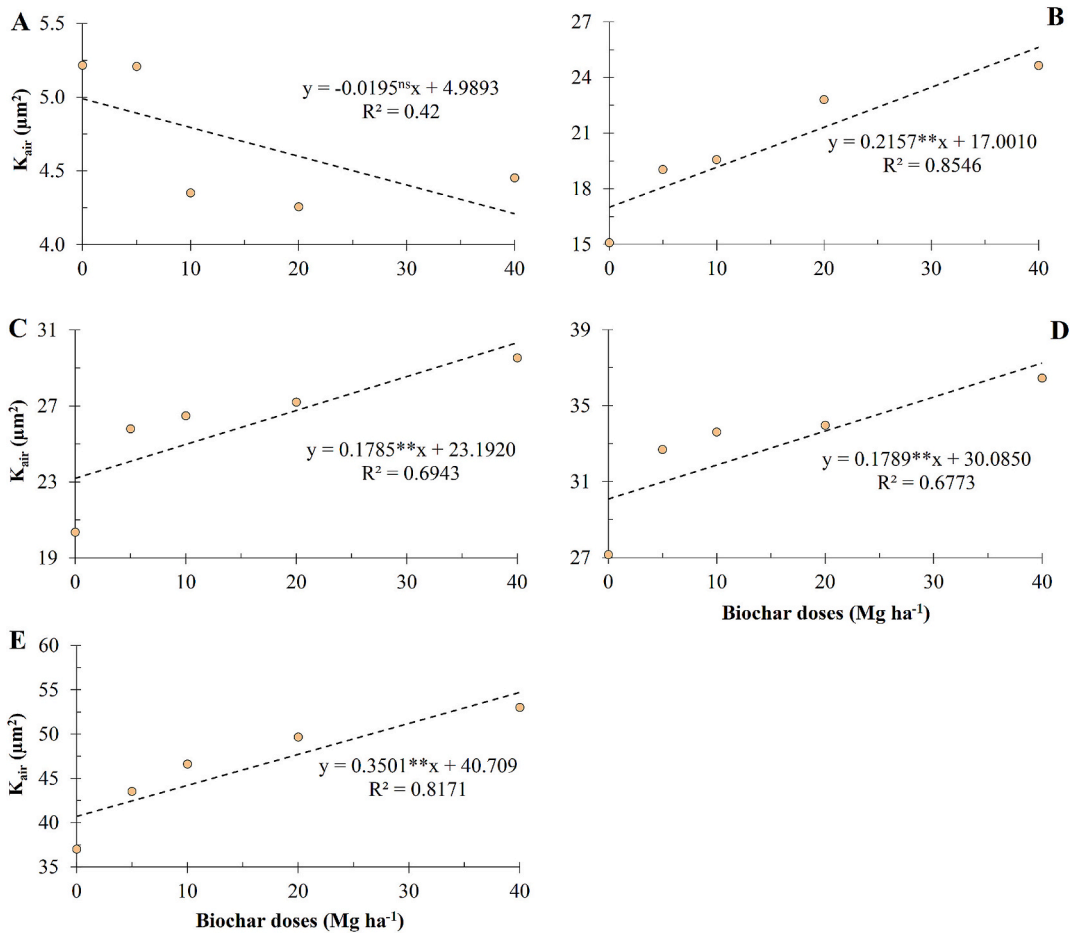

Fig. 7. Regression between air permeability (K_{air}) and biochar doses for each evaluated matric potential, namely: −2 kPa (A), −6 kPa (B), −10 kPa (C), −33 kPa (D), and − 100 kPa (E) (n = 5). *Significant at 5 % probability; **Significant at 1 % probability; [ns]Not significant.

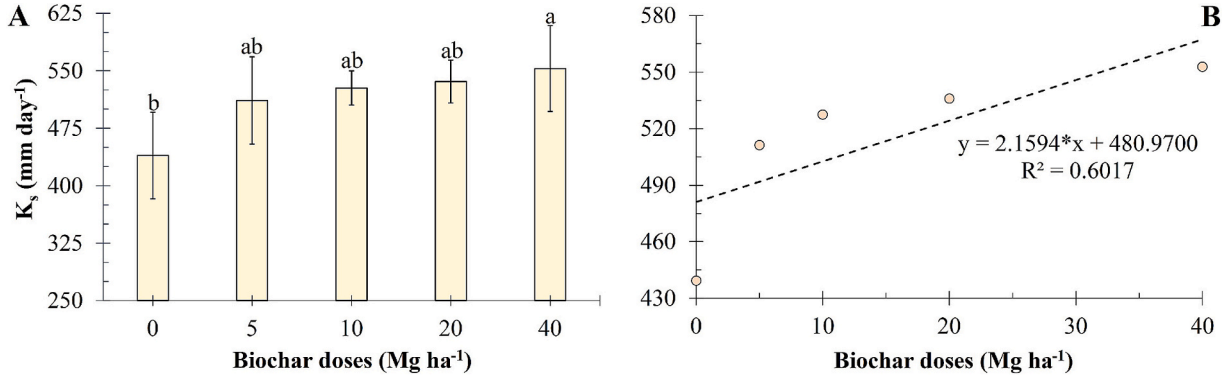

Fig. 8. Saturated hydraulic conductivity (K_s) as a function of biochar doses (A). Regression between K_s and biochar doses (B) (n = 5). Means followed by the same letter do not differ according to the Tukey test at a 5 % significance level. The bars represent the standard error of the mean. *Significant at the 5 % probability level.

macroporosity and pore network connectivity provided by the biochar. Nonetheless, it is valid to infer that the natural aging process of biochar may alter particle size and potentially lead to the occlusion of pores of other size ranges.

Granulometric analysis of the cashew-residue biochar (Table 2) indicates that ~97.5 % of particles exceed 0.25 mm (250 µm) and even the smallest fraction (8.54 %) spans 105–250 µm; since macropores ≥150 µm lie well within this range, these biochar fragments are mechanically capable of lodging in and partially occluding these pores, thereby explaining the observed increase in pore blockage at this specific diameter.

In this way, small biochar particles can settle into the spaces between larger soil particles, decreasing pore dimensions and modifying the geometry of the pore network (Liu et al., 2017). Although this effect is more noticeable in coarse-textured sandy soils (Edeh and Mašek, 2022; Zhang et al., 2024a; Zhu et al., 2025), it is also possible for this type of process to occur in finer-textured soils, such as the studied horizon (sandy clay). Therefore, the appropriate selection of biochar particle size is essential to optimize the agronomic and environmental benefits of its application, taking into account the specific soil characteristics and

management objectives (Lima et al., 2021).

In this context, a comprehensive investigation should not be overlooked. Employing more advanced analytical techniques — such as computed tomography or micromorphology —is essential to validate the current findings and to prevent potential long-term detrimental effects on the soil, such as reduced permeability and the onset of erosive processes (Baveye, 2023).

4.3. Integrated air and water flow enhancements

Gas exchanges between soil and the atmosphere are crucial for renewing soil oxygen (O_2) supplies and for the removal of carbon dioxide (CO_2) produced by plant and soil organism respiration (Lal and Shukla, 2004). Inadequate gas exchange can lead to CO_2 toxicity for plants even before O_2 depletion becomes a problem (Hillel, 2004). In cohesive horizons, the reduction in total porosity with increased soil bulk density impairs both water and air fluxes (Marques et al., 2021), negatively impacting plant growth. Therefore, the application of the tested biochar, which increases K_{air} (Fig. 6), presents a promising alternative for enhancing the physical quality of these horizons by facilitating gas exchange.

The threshold value of K_{air} necessary for the proper development of most plants is 1 μm^2 of available area (McQueen and Shepherd, 2002). This ensures effective removal of CO_2 and renewal of O_2 in the soil. Although K_{air} values were consistently above 1 μm^2 across all scenarios (Fig. 6), the highest values were observed with biochar treatments, with K_{air} increasing as the biochar dose increased in all matric potentials evaluated, except at conditions closest to saturation ($\Psi_m = -2$ *kPa*, Fig. 7A). This increase results from biochar-enhanced macroporosity, as its electrically active particles promote flocculation and aggregation, thereby boosting total porosity — especially of air-conducting pores (macropores) (Nascimento et al., 2023). Although drying–wetting cycles can generate macropores through shrink–swell cracking in soils rich in 2:1 expandable clays (e.g., smectite) (Ahlersmeyer et al., 2025; Yang et al., 2025), such natural mechanisms are subdued in our 1:1 kaolinitic horizon due to its low shrinkage potential. Consequently, the improvements in soil structure and K_{air} documented here are attributable predominantly to the physical effects of biochar amendment rather than to inherent shrink–swell dynamics.

However, it is important to note that air permeability reflects only the convective component of gas transport in soils (Ball and Schjønning, 2002). Therefore, while increased K_{air} values suggest improved air-filled porosity and pore connectivity, they do not capture diffusive gas movement, which is the dominant mechanism under unsaturated conditions (Reichardt and Timm, 2020).

Biochar application resulted in greater pore connectivity (Fig. 4). Consequently, soil pores formed a more continuous network, improving gas exchange processes and soil structural quality (Alencar et al., 2016), as evidenced by the higher air permeability values observed. However, in the evaluation of the pore network in a cohesive soil using micromorphology techniques, it was found that pores in cohesive horizons are predominantly oriented horizontally (Lima et al., 2006). In that regard, our measurement of K_{air} represents a bulk transport property and does not distinguish flow direction.

The only instance where a trend of reduced K_{air} with increased biochar dose was observed occurred under near-saturated conditions ($\Psi_m = -2$ kPa, Fig. 7A), although this trend was not statistically significant. We included −2 kPa alongside −6, −10, −33 and − 100 kPa measurements to assess air permeability from near-saturation through progressively drier states. Given that biochar particles can obstruct pores ≥150 μm, this near-saturated test may be particularly sensitive to partial occlusion, consistent with the observed increase in blocked porosity at higher biochar doses (Fig. 5B).

In terms of K_s, this attribute is controlled by the geometry and distribution of pores by size (Edeh et al., 2020). As previously reported, there was a trend of increasing macropore proportion in response to the increase in the dose of the evaluated biochar (Fig. 3) – and macropores are conduits for water and air (Reichardt and Timm, 2020). Furthermore, the soil pores became part of a more continuous pore network (Fig. 4), positively affecting not only gas flux (Fig. 6) but also the ability to conduct water, i.e., its hydraulic conductivity (Fig. 8) – which is maximal in saturated soil (Almeida et al., 2018).

The increase in K_s in clayey and/or compacted soils that received biochar application is well documented in the literature, often related to an increase in macroporosity (Alghamdi, 2018; Edeh et al., 2020; Santos, 2021). While certain biochars may exhibit hydrophobic properties that increase water repellency and reduce hydraulic conductivity (Blanco-Canqui, 2017), the cashew-residue biochar used here is hydrophilic (Fregolente et al., 2023). This hydrophilicity is reflected in the similarity of the soil-water retention curves between the control and biochar treatments (Fig. 3).

In cohesive horizons, a decrease in total porosity with an increase in soil density results in impaired water and air fluxes (Nascimento et al., 2024), hindering plant development. Thus, the application of cashew bagasse biochar, by increasing K_s, represents a viable alternative for improving physical quality in cohesive horizons, as this variable has a direct influence on water infiltration and drainage processes (Gonçalves and Libardi, 2013) and, therefore, plays a key role in the hydrological cycle (Chow et al., 2013).

4.4. Balancing connectivity gains and pore-blockage

These results highlight the potential of cashew-residue biochar as a soil conditioner to improve macroporosity, pore continuity, plant-available water, gas exchange, and saturated hydraulic conductivity in cohesive soil horizons. However, at the highest application rates (20–40 Mg ha^{-1}), the same biochar particles that enhance pore connectivity can also partially occlude macropores ≥150 μm, causing localized pore blockage. Thus, while 20–40 Mg ha^{-1} maximizes overall soil physical quality under controlled conditions, these rates involve a trade-off between improved connectivity and potential flow impedance.

Although the improvements in pore connectivity and water–air dynamics at higher biochar doses are evident, the observed partial blockage of macropores ≥150 μm underscores a limitation of excessive biochar application. Such occlusion may locally restrict flow paths, potentially reducing water infiltration and impairing root aeration under field conditions. These findings emphasize that biochar amendment should not follow a “more is better” approach but rather require careful optimization to balance benefits and drawbacks. Identifying the optimal dose is critical for enhancing soil structure without compromising key hydraulic and aeration properties. Consequently, site-specific calibration and tailored application strategies are necessary to ensure sustainable improvements in soil functionality.

Before making field recommendations, it is essential to (i) validate these findings under heterogeneous field conditions, (ii) quantify the net effects of pore blockage versus connectivity on crop performance, and (iii) develop economically and technically feasible application methods that optimize biochar placement. Future research should also examine biochar aging effects on particle size and pore dynamics to support sustainable and scalable implementation.

It is important to note that all measurements were performed under controlled laboratory conditions using homogenized soil–biochar mixtures; thus, the uniform biochar distribution in our soil rings may have amplified its effects compared to field applications, where spatial variability in biochar placement could diminish these benefits. Nonetheless, this laboratory-based approach provides valuable mechanistic insights into biochar–soil interactions. Therefore, field trials are needed to confirm the applicability of the 20–40 Mg ha^{-1} rates under real-world heterogeneity.

Additionally, this study was conducted using disturbed soil samples packed into rings under controlled laboratory settings. As a result, the observed responses may not fully represent the behavior of cohesive

soils under natural field conditions, where intact soil structure, spatial heterogeneity, and environmental interactions can substantially influence biochar effects. This limitation highlights the necessity of field validation to capture the complexity and variability of soils, ensuring the applicability and reliability of management recommendations.

Finally, it is important to acknowledge that plant growth was not assessed in this study. The absence of live plants limits the direct evaluation of agronomic outcomes such as root development, nutrient uptake, and crop productivity, which are crucial for practical applications. Hence, future research should incorporate plant growth experiments under both controlled and field conditions to comprehensively evaluate the agronomic and environmental effects of cashew-residue biochar amendments in cohesive soils.

5. Conclusions

The application of cashew-residue biochar markedly enhanced soil macroporosity, pore connectivity, air permeability, and saturated hydraulic conductivity in cohesive horizons, validating our initial hypothesis and demonstrating clear benefits for soil physical quality and management efficiency. Rates of 20–40 Mg ha^{-1} provided the greatest improvements in soil structure and functionality; however, partial occlusion of macropores ($\geq$150 μm) at these doses highlighted a trade-off between enhanced pore connectivity and localized flow restriction.

This study provides novel insights into the use of cashew-residue biochar for improving the physical quality of cohesive soils, a soil type that has received limited attention in biochar research. By demonstrating significant short-term improvements in key soil physical properties, these findings advance the understanding of biochar's role in mitigating compaction-related constraints and support the development of management strategies for cohesive soils.

Before recommending 20–40 Mg ha^{-1} for field applications, further research is required to (i) validate these laboratory findings under spatially heterogeneous conditions, (ii) quantify the net effects of pore blockage versus connectivity gains on plant performance, and (iii) develop cost-effective, technically viable application strategies.

Finally, because this was a short-term incubation study, future work should assess long-term biochar aging, including its effects on particle stability, pore network dynamics, and the persistence of soil physical improvements, to ensure sustainable, field-scale adoption of this amendment.

CRediT authorship contribution statement

Jaedson Cláudio Anunciato Mota: Writing – review & editing, Writing – original draft, Visualization, Validation, Supervision, Methodology, Investigation, Funding acquisition, Formal analysis, Data curation, Conceptualization. **Emanuela Barbosa dos Santos:** Writing – review & editing, Writing – original draft, Methodology, Investigation, Formal analysis. **Alexandre dos Santos Queiroz:** Writing – review & editing, Writing – original draft, Visualization, Methodology, Investigation, Formal analysis. **Odair Pastor Ferreira:** Writing – review & editing, Writing – original draft, Visualization, Supervision, Methodology, Investigation, Conceptualization. **Antônio Gomes de Souza Filho:** Writing – review & editing, Writing – original draft, Supervision, Resources, Project administration, Funding acquisition. **Laís Gomes Fregolente:** Writing – review & editing, Writing – original draft, Visualization, Validation, Methodology, Investigation, Formal analysis. **Francisca Gleiciane da Silva:** Writing – review & editing, Writing – original draft, Visualization, Supervision, Methodology, Investigation. **Arthur Prudêncio de Araujo Pereira:** Writing – review & editing, Writing – original draft, Supervision, Methodology, Investigation, Conceptualization. **Helon Hébano de Freitas Sousa:** Writing – review & editing, Writing – original draft, Supervision, Methodology, Investigation, Conceptualization. **Mirian Cristina Gomes Costa:** Writing – review & editing, Writing – original draft, Visualization, Supervision, Resources, Project administration, Methodology, Investigation, Data curation, Conceptualization. **Ícaro Vasconcelos do Nascimento:** Writing – review & editing, Writing – original draft, Visualization, Validation, Methodology, Investigation, Formal analysis, Data curation, Conceptualization.

Declaration of generative AI and AI-assisted technologies in the writing process

While preparing this manuscript, the authors employed OpenAI's ChatGPT as a language-editing tool. After utilizing this service, the authors reviewed and revised the content as necessary and accepted full responsibility for the content of the publication.

Declaration of competing interest

The authors declare that they have no known competing financial interests or personal relationships that could have appeared to influence the work reported in this paper.

Acknowledgments

This study was supported by the Agricultural Chief Scientist Program of the Government of the State of Ceará (Agreement 14/2022 SDE/ADECE/FUNCAP and Process 08126425/2020/FUNCAP). Additional support was received from the Financial Agency for Studies and Projects (FINEP), grant number 0122017200. Í.V. Nascimento and F. G. Silva thank the Federal Agency for Support and Evaluation of Graduate Education (CAPES) for their scholarships. L.G. Fregolente acknowledges the Ceará Foundation for Support to Scientific and Technological Development (FUNCAP) for the scholarship. J.C.A. Mota, M.C.G. Costa, A.P.A. Pereira, and O.P. Ferreira express their gratitude to CNPq (National Council for Scientific and Technological Development) for their research grants (Processes: 303524/2022–7; 305907/2019–0; 305231/2023–5; 310821/2022–3; and 409205/2023–0).

Data availability

The data that has been used is confidential.

References

Ahlersmeyer, A., Clay, D., Kovács, P., Osterloh, K., Rekabdarkolaee, H.M., Clark, J., 2025. Relationships among soil test potassium forms influenced by clay mineralogy. Soil Sci. Soc. Am. J. 89. https://doi.org/10.1002/saj2.70015.

Ahuja, L.R., Naney, J.W., Green, R.E., Nielsen, D.R., 1984. Macroporosity to characterize spatial variability of hydraulic conductivity and effects of land management. Soil Sci. Soc. Am. J. 48, 699–702. https://doi.org/10.2136/sssaj1984.03615995004800040001x.

Alencar, T.L., Chaves, A.F., Freire, A.G., Assis Júnior, R.N., Mota, J.C.A., 2016. Liquid bovine biofertilizer and cultivation effects on the porosity of a typic haplocambids as a function of cultivation and dose. Rev. Bras. Cienc Solo 40. https://doi.org/10.1590/18069657rbcs20150307.

Alghamdi, A.G., 2018. Biochar as a potential soil additive for improving soil physical properties—a review. Arab. J. Geosci. 11, 766. https://doi.org/10.1007/s12517-018-4056-7.

Almeida, K.S.S.A., Souza, L.S., Paz, V.P.S., Silva, F.T.S., Santos, D.N., Pereira, J.S.L., 2018. Variabilidade espacial da condutividade hidráulica do solo saturado em Latossolo Amarelo distrocoeso, no Município de Cruz das Almas. IRRIGA 22, 259–274. https://doi.org/10.15809/irriga.2017v22n1p259-274.

Arshad, M.A., Martin, S., 2002. Identifying critical limits for soil quality indicators in agro-ecosystems. Agric. Ecosyst. Environ. 88, 153–160. https://doi.org/10.1016/S0167-8809(01)00252-3.

Ball, B.C., Schjønning, P., 2002. 4.4 air permeability. In: Jacob, H., Dane, G., Toop, C. (Eds.), Methods of Soil Analysis: Part 4 Physical Methods. Soil Science Society of America, Inc, Madison, pp. 1141–1158. https://doi.org/10.2136/sssabookser5.4.c46.

Baveye, P.C., 2023. Unknown economic costs of biochar applications to soils: they should be considered in the on-going debate. Resour. Conserv. Recycl. 192, 106911. https://doi.org/10.1016/j.resconrec.2023.106911.

Blanco-Canqui, H., 2017. Biochar and soil physical properties. Soil Sci. Soc. Am. J. 81, 687–711. https://doi.org/10.2136/sssaj2017.01.0017.

Campos, M., Penn, C.J., Gonzalez, J.M., Alexandre Costa Crusciol, C., 2022. Effectiveness of deep lime placement and tillage systems on aluminum fractions and soil chemical attributes in sugarcane cultivation. Geoderma 407, 115545. https://doi.org/10.1016/j.geoderma.2021.115545.

Chow, V.T., Maidment, D.R., Mays, L.W., 2013. Applied Hydrology, 2nd ed. In: McGraw-Hill series in water resources and environmental engineering. McGraw-Hill Professional, United States.

Corrêa, M.M., de Araújo Filho, J.C., Schaefer, Carlos E.G.R., Ker, J.C., 2023. Soils of the coastal tablelands under Atlantic Forest (Tabuleiros Costeiros). In: Schaefer, C.E.G.R. (Ed.), The Soils of Brazil, World Soils Book Series. Springer, Charm, pp. 221–238. https://doi.org/10.1007/978-3-031-19949-3_8.

Doran, J.W., Parkin, T.B., 1994. Defining and assessing soil quality. In: Doran, J.W., Colemam, D.C., Bezdicek, D.F., Stewart, B.A. (Eds.), Defining Soil Quality for a Sustainable Environment. Soil Science Society of America, Madison, pp. 1–21. https://doi.org/10.2136/sssaspecpub35.c1.

Dourado-Neto, D., Nielsen, D.R., Hopmans, J.W., Reichardt, K., Bacchi, O.O.S., 2000. Software to model soil water retention curves (SWRC, version 2.00). Sci. Agric. 57, 191–192. https://doi.org/10.1590/S0103-90162000000100031.

Duarte, S.J., Glaser, B., Cerri, C.P., 2019. Effect of biochar particle size on physical, hydrological and chemical properties of loamy and Sandy tropical soils. Agronomy 9, 165. https://doi.org/10.3390/agronomy9040165.

Edeh, I.G., Mašek, O., 2022. The role of biochar particle size and hydrophobicity in improving soil hydraulic properties. Eur. J. Soil Sci. 73. https://doi.org/10.1111/ejss.13138.

Edeh, I.G., Mašek, O., Buss, W., 2020. A meta-analysis on biochar's effects on soil water properties – new insights and future research challenges. Sci. Total Environ. 714, 136857. https://doi.org/10.1016/j.scitotenv.2020.136857.

Elkhlifi, Z., Iftikhar, J., Sarraf, M., Ali, B., Saleem, M.H., Ibranshahib, I., Bispo, M.D., Meili, L., Ercisli, S., Torun Kayabasi, E., Alemzadeh Ansari, N., Hegedűsová, A., Chen, Z., 2023. Potential role of biochar on capturing soil nutrients, carbon sequestration and managing environmental challenges: a review. Sustainability 15, 2527. https://doi.org/10.3390/su15032527.

Fregolente, L.G., Rodrigues, M.T., Oliveira, N.C., Araújo, B.S., Nascimento, Í.V., Souza Filho, A.G., Paula, A.J., Costa, M.C.G., Mota, J.C.A., Ferreira, O.P., 2023. Effects of chemical aging on carbonaceous materials: stability of water-dispersible colloids and their influence on the aggregation of natural-soil colloid. Sci. Total Environ. 903, 166835. https://doi.org/10.1016/j.scitotenv.2023.166835.

Gonçalves, A.D.M.A., Libardi, P.L., 2013. Análise da determinação da condutividade hidráulica do solo pelo método do perfil instantâneo. Rev. Bras. Cienc Solo 37, 1174–1184. https://doi.org/10.1590/S0100-06832013000500007.

Hillel, D., 2004. Introduction to Environmental Soil Physics. Elsevier. https://doi.org/10.1016/B978-0-12-348655-4.X5000-X.

IUSS Working Group WRB, 2022. World Reference Base for Soil Resources. International Soil Classification System for Naming Soils and Creating Legends for Soil Maps, 4th ed. Vienna, Austria.

Jorge, R.F., Corá, J.E., Barbosa, J.C., 2010. Número mínimo de tensões para determinação da curva característica de retenção de água de um latossolo vermelho eutrófico sob sistema de semeadura direta. Rev. Bras. Cienc Solo 34, 1831–1840. https://doi.org/10.1590/s0100-06832010000600007.

Karlen, D.L., Mausbach, M.J., Doran, J.W., Cline, R.G., Harris, R.F., Schuman, G.E., 1997. Soil quality: a concept, definition, and framework for evaluation (a guest editorial). Soil Sci. Soc. Am. J. 61, 4–10. https://doi.org/10.2136/sssaj1997.03615995006100010001x.

Kirkham, D., 1947. Field method for determination of air permeability of soil in its undisturbed state. Soil Sci. Soc. Am. J. 11, 93–99.

Klute, A., 1986. Water retention: Laboratory methods. In: Klute, Arnold (Ed.), Methods of Soil Analysis: Part 1 Physical and Mineralogical Methods. Soil Science Society of America, Madison, pp. 635–662. https://doi.org/10.2136/sssabookser5.1.2ed.c26.

Koppen, W., 1918. Klassifikation der klimate nach Temperatur, Niederschlag und Jahreslauf. Petermanns Geogr. Mitt. 64, 193–248.

Lal, R., 2016. Soil health and carbon management. Food Energy Secur. 5, 212–222. https://doi.org/10.1002/fes3.96.

Lal, R., Shukla, M.K., 2004. Principles of Soil Physics. Marcel Dekker, New York.

Letey, J., 1985. In: Stewart, B.A. (Ed.), Relationship between Soil Physical Properties and Crop Production. Springer, New York, pp. 277–294. https://doi.org/10.1007/978-1-4612-5046-3_8.

Li, S., Tasnady, D., 2023. Biochar for soil carbon sequestration: current knowledge, mechanisms, and future perspectives. C (Basel) 9, 67. https://doi.org/10.3390/c9030067.

Lima, H.V., Silva, A.P., Santos, M.C., Cooper, M., Romero, R.E., 2006. Micromorphology and image analysis of a hardsetting Ultisol (Argissolo) in the state of Ceará (Brazil). Geoderma 132, 416–426. https://doi.org/10.1016/j.geoderma.2005.06.006.

Lima, J.R.S., Goes, M.C.C., Antonino, A.C.D., Medeiros, É.V., Duda, G.P., Leite, M.C.B.S., Silva, V.P., Souza, B.L.L., Hammecker, C., 2021. Biochar enhances Acrisol attributes and yield of bean in Brazilian tropical dry region. Acta Agric. Scand. Sect. B Soil Plant Sci. 71, 674–682. https://doi.org/10.1080/09064710.2021.1937691.

Liu, Z., Dugan, B., Masiello, C.A., Gonnermann, H.M., 2017. Biochar particle size, shape, and porosity act together to influence soil water properties. PLoS One 12, e0179079. https://doi.org/10.1371/journal.pone.0179079.

Lopes, A.S., Queiroz, A.S., Nascimento, Í.V., Oliveira, L.S., Almeida, B.G., Araújo Filho, J. C., Souza, L.S., Silva, M.B., Romero, R.E., Silva, F.G., Costa, M.C.G., Mota, J.C.A., 2024. Proposal of a revision scale of the degree of cohesion and tensile strength to aid in the diagnosis of the cohesive character in soils. Catena (Amst.) 245, 108284. https://doi.org/10.1016/j.catena.2024.108284.

Luo, L., Wang, J., Lv, J., Liu, Z., Sun, T., Yang, Y., Zhu, Y.-G., 2023. Carbon sequestration strategies in soil using biochar: advances, challenges, and opportunities. Environ. Sci. Technol. 57, 11357–11372. https://doi.org/10.1021/acs.est.3c02620.

Marques, E.S., Mota, J.C.A., Lacerda, C.F., Silva, F.G., Romero, R.E., 2021. Gas exchange in maize as a function of aeration porosity in a cohesive soil. Rev. Ciênc. Agron. 52. https://doi.org/10.5935/1806-6690.20210035.

McQueen, D.J., Shepherd, T.G., 2002. Physical changes and compaction sensitivity of a fine-textured, poorly drained soil (Typic Endoaquept) under varying durations of cropping, Manawatu Region, New Zealand. Soil Tillage Res. 63, 93–107. https://doi.org/10.1016/S0167-1987(01)00231-8.

Mendes, J.S., Fernandes, J.D., Chaves, L.H.G., Guerra, H.O.C., Tito, G.A., Brito, C.I., 2021. Chemical and physical changes of soil amended with biochar. Water Air Soil Pollut. 232, 338. https://doi.org/10.1007/s11270-021-05289-8.

Menezes, A.S., Alencar, T.L., Assis Júnior, R.N., Toma, R.S., Romero, R.E., Costa, M.C.G., Cooper, M., Mota, J.C.A., 2018. Functionality of the porous network of Bt horizons of soils with and without cohesive character. Geoderma 313, 290–297. https://doi.org/10.1016/j.geoderma.2017.11.005.

Mota, J.C.A., Menezes, A.S., Nascimento, C.D.V., Alencar, T.L., Assis Júnior, R.N., Toma, R.S., Romero, R.E., Costa, M.C.G., Cooper, M., 2018. Pore shape, size distribution and orientation in Bt horizons of two Alfisols with and without cohesive character from Brazil. Geoderma Reg. 15, e00197. https://doi.org/10.1016/j.geodrs.2018.e00197.

Mullins, C.E., MacLeod, D.A., Northcote, K.H., Tisdall, J.M., Young, I.M., 1990. Hardsetting Soils: Behavior, Occurrence, and Management, pp. 37–108. https://doi.org/10.1007/978-1-4612-3322-0_2.

Nascimento, Í.V., Alencar, T.L., Santos, C.L.A., Assis Júnior, R.N., Mota, J.C.A., 2018a. Effect of sample re-saturation on soil-water characteristic curve. Rev. Caatinga 31, 446–454. https://doi.org/10.1590/1983-21252018v31n221rc.

Nascimento, Í.V., Assis Júnior, R.N., Araújo, J.C., Alencar, T.L., Freire, A.G., Lobato, M.G. R., Silva, C.P., Mota, J.C.A., Nascimento, C.D.V., 2018b. Estimation of van Genuchten equation parameters in laboratory and through inverse modeling with Hydrus-1D. J. Agric. Sci. 10, 102. https://doi.org/10.5539/jas.v10n3p102.

Nascimento, Í.V., Fregolente, L.G., Pereira, A.P.A., Nascimento, C.D.V., Mota, J.C.A., Ferreira, O.P., Sousa, H.H.F., Silva, D.G.G., Simões, L.R., Souza Filho, A.G., Costa, M. C.G., 2023. Biochar as a carbonaceous material to enhance soil quality in drylands ecosystems: a review. Environ. Res. 233, 116489. https://doi.org/10.1016/j.envres.2023.116489.

Nascimento, Í.V., Santos, E.B., Lopes, A.S., Queiroz, A.S., Teixeira Filho, C.D., Romero, R. E., Costa, M.C.G., Ferreira, O.P., Souza Filho, A.G., Fregolente, L.G., Silva, F.G., Pereira, A.P.A., Sousa, H.H.F., Sobucki, V., Reichert, J.M., Mota, J.C.A., 2024. Biochar from cashew residue enhances silicon adsorption and reduces cohesion and mechanical resistance at meso- and micro-structural scales of soil with cohesive character. Soil Tillage Res. 241, 106101. https://doi.org/10.1016/j.still.2024.106101.

National Committee on Soil and Terrain, 2009. Australian Soil and Land Survey Field Handbook, 3rd ed. CSIRO Publishing, Clayton. https://doi.org/10.1071/9780643097117.

Neves, C.M.N., Silva, M.L.N., Curi, N., Cardoso, E.L., Macedo, R.L.G., Ferreira, M.M., Souza, F.S., 2007. Atributos indicadores da qualidade do solo em sistema agrossilvopastoril no noroeste do estado de Minas Gerais. Sci. For. 74, 45–53.

Ning, T., Liu, Z., Hu, H., Li, G., Kuzyakov, Y., 2022. Physical, chemical and biological subsoiling for sustainable agriculture. Soil Tillage Res. 223, 105490. https://doi.org/10.1016/j.still.2022.105490.

Oliveira, L.G.L., Ipiranga, A.S.R., 2011. Evidences of the sustainable innovation in the cashew agribusiness context in Ceará - Brazil. Rev. Admin. Mackenzie 12, 122–150. https://doi.org/10.1590/S1678-69712011000500006.

Oliveira, L.S., Maia, R.N., Assis Júnior, R.N., Romero, R.E., Costa, M.C.G., Alencar, T.L., Mota, J.C.A., 2020. Tensile strength values for the degrees of soil consistency using human perception and TS-soil device. Catena (Amst.) 190, 104541. https://doi.org/10.1016/j.catena.2020.104541.

Queiroz, A.S., Dias, C.T.S., Lopes, A.S., Nascimento, Í.V., Oliveira, L.S., Almeida, B.G., Araújo Filho, J.C., Souza, L.S., Silva, M.B., Romero, R.E., Toma, R.S., Sousa, H.H.F., Mota, J.C.A., 2023. Water content as a deterministic factor in the assessment of cohesive character in soils of coastal tablelands (Northeast, Brazil). Geoderma Reg. 32, e00600. https://doi.org/10.1016/j.geodrs.2022.e00600.

Razzaghi, F., Obour, P.B., Arthur, E., 2020. Does biochar improve soil water retention? A systematic review and meta-analysis. Geoderma 361, 114055. https://doi.org/10.1016/j.geoderma.2019.114055.

Reichardt, K., Timm, L.C., 2020. Soil, Plant and Atmosphere. Springer International Publishing, Cham. https://doi.org/10.1007/978-3-030-19322-5.

Santos, E.B., 2021. Comportamento físico e hídrico de solos em interação com carvão vegetal (Doctorate thesis). Federal University of Ceará, Fortaleza.

Santos, H.G., Jacomine, P.K.T., Anjos, L.H.C., Oliveira, V.A., Lumbreras, J.F., Coelho, M. R., Almeida, J.A., Araújo Filho, J.C., Oliveira, J.C., Cunha, T.J.F., Jarbas Ferreira Cunha, T., 2018. Sistema Brasileiro de Classificação de Solos, 5th ed. Embrapa, Brasília.

Seifu, W., Elias, E., 2018. Soil quality attributes and their role in sustainable agriculture: a review. Int. J. Plant Soil Sci. 26, 1–26. https://doi.org/10.9734/ijpss/2018/41589.

Silva, A.P., Leão, T.P., Tormena, C.A., Gonçalves, A.C.A., 2009. Determinação da permeabilidade ao ar em amostras indeformadas de solo pelo método da pressão decrescente. Rev. Bras. Cienc Solo 33, 1535–1545. https://doi.org/10.1590/S0100-06832009000600003.

Silveira, L.R., Brito, A.S., Mota, J.C.A., Moraes, S.O., Libardi, P.L., 2011. Sistema de aquisição de dados para equipamento de medida da permeabilidade intrínseca do solo ao ar. Rev. Bras. Cienc Solo 35, 429–436. https://doi.org/10.1590/S0100-06832011000200012.

Singh, H., Northup, B.K., Rice, C.W., Prasad, P.V.V., 2022. Biochar applications influence soil physical and chemical properties, microbial diversity, and crop productivity: a meta-analysis. Biochar 4, 8. https://doi.org/10.1007/s42773-022-00138-1.

Torres, G.N., Amorim, R.S.S., Raimo, L.L., Faria, O.C.O., Couto, E.G., 2024. Water retention in sandy soils of different origins with the addition of biochar. Rev. Caatinga 37. https://doi.org/10.1590/1983-21252024v3711792rc.

van Genuchten, M.T., 1980. A closed-form equation for predicting the hydraulic conductivity of unsaturated soils. Soil Sci. Soc. Am. J. 44, 892–898. https://doi.org/10.2136/sssaj1980.03615995004400050002x.

van Lier, Q.J., Pinheiro, E.A.R., 2018. An alert regarding a common misinterpretation of the Van Genuchten α parameter. Rev. Bras. Cienc Solo 42. https://doi.org/10.1590/18069657rbcs20170343.

Varkolu, M., Gundekari, S., Omvesh Palla, V.C.S., Kumar, P., Bhattacharjee, S., Vinodkumar, T., 2025. Recent advances in biochar production, characterization, and environmental applications. Catalysts 15, 243. https://doi.org/10.3390/catal15030243.

Verheijen, F.G.A., Zhuravel, A., Silva, F.C., Amaro, A., Ben-Hur, M., Keizer, J.J., 2019. The influence of biochar particle size and concentration on bulk density and maximum water holding capacity of sandy vs sandy loam soil in a column experiment. Geoderma 347, 194–202. https://doi.org/10.1016/j.geoderma.2019.03.044.

Vieira, J.M., 2013. Contribuição de compostos de baixa cristalinidade e ciclos de umedecimento e secagem na gênese do caráter coeso em solos do Ceará (Master's Thesis). Federal University of Ceará, Fortaleza.

Wang, J., Wang, S., 2019. Preparation, modification and environmental application of biochar: a review. J. Clean. Prod. 227, 1002–1022. https://doi.org/10.1016/j.jclepro.2019.04.282.

Yang, X., Zhang, S., Ju, M., Liu, L., 2019. Preparation and modification of biochar materials and their application in soil remediation. Appl. Sci. 9, 1365. https://doi.org/10.3390/app9071365.

Yang, F., Zhao, Y., Dong, H., Wang, H., Niu, W., Zhao, Z., Song, F., Tan, H., 2025. Mechanical and microscopic characterization of expansive soils modified by water-soluble polymers. Sci. Rep. 15, 2315. https://doi.org/10.1038/s41598-025-85395-3.

Youngs, E.G., 2000. Hydraulic conductivity of satured soils. In: Smith, K.A., Mullings, C. E. (Eds.), Soil Analysis: Physical Methods. Marcel Dekker, New York, pp. 141–182.

Zhang, P., Chang, F., Huo, L., Yao, Z., Luo, J., 2024a. Impacts of biochar pyrolysis temperature, particle size, and application rate on water retention of loess in the semiarid region. Water (Basel) 17, 69. https://doi.org/10.3390/w17010069.

Zhang, K., Wei, H., Chai, Q., Li, L., Wang, Y., Sun, J., 2024b. Biological soil conditioner with reduced rates of chemical fertilization improves soil functionality and enhances rice production in vegetable-rice rotation. Appl. Soil Ecol. 195, 105242. https://doi.org/10.1016/j.apsoil.2023.105242.

Zhu, Z., Zhang, Y., Tao, W., Zhang, X., Xu, Z., Xu, C., 2025. The biological effects of biochar on soil's physical and chemical characteristics: a review. Sustainability 17, 2214. https://doi.org/10.3390/su17052214.

Zong, Y., Chen, D., Lu, S., 2014. Impact of biochars on swell–shrinkage behavior, mechanical strength, and surface cracking of clayey soil. J. Plant Nutr. Soil Sci. 177, 920–926. https://doi.org/10.1002/jpln.201300596.